Science of the Total Environment 777 (2021) 146185

Contents lists available at ScienceDirect

Science of the Total Environment

journal homepage: www.elsevier.com/locate/scitotenv

Morphological and chemical properties of fibrous antigorite from lateritic deposit of New Caledonia in view of hazard assessment

Jasmine R. Petriglieri [a,b,*], Christine Laporte-Magoni [c], Emma Salvioli-Mariani [d], Simona Ferrando [a,e], Maura Tomatis [a,b], Bice Fubini [a,b], Francesco Turci [a,b]

[a] "G. Scansetti" Interdepartmental Centre for Studies on Asbestos and Other Toxic Particulates, University of Torino, Via Pietro Giuria 7, I-10125 Torino, Italy
[b] Department of Chemistry, University of Torino, Via Pietro Giuria 7, I-10125 Torino, Italy
[c] Institute of Exact and Applied Sciences, Université de la Nouvelle Calédonie, Campus de Nouville, BP R4-98851 Nouméa Cedex, New Caledonia, France
[d] Department of Chemistry, Life Sciences and Environmental Sustainability, University of Parma, Parco Area delle Scienze 157/A, I-43124 Parma, Italy
[e] Department of Earth Sciences, University of Torino, Via Valperga Caluso 35, I-10125 Torino, Italy

HIGHLIGHTS

- Antigorite often occurs in the Ni-rich lateritic ores in New Caledonia.
- Antigorite from New Caledonia has a fibrous asbestos-like morphology.
- Supergene alteration affects bulk chemistry of antigorite from lateritic deposits.
- Weathering prompts the mechanical disaggregation of altered antigorites.

GRAPHICAL ABSTRACT

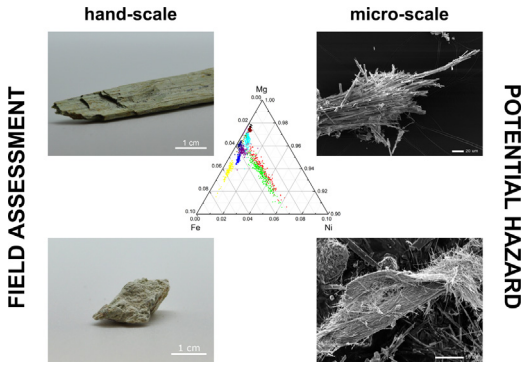

ARTICLE INFO

Article history:
Received 18 December 2020
Received in revised form 11 February 2021
Accepted 24 February 2021
Available online 3 March 2021

Editor: Daqiang Yin

Keywords:
Fibrous antigorite
NOA
EMP
Supergene alteration
Weathering
Asbestos

ABSTRACT

Exposure to natural occurrences of asbestos (NOA) and other potentially hazardous elongated mineral particles (EMPs) may pose a risk to human health and the environment. Weathering forces and anthropic activities may alter the cohesion of NOA-bearing outcrops and disperse EMPs in air, water, and soil. The current paradigm for fibre toxicity indicates that morphology and crystal chemistry are key parameters in determining the toxicological properties of a mineral. This work aims to assess and discuss the impact of sub-tropical supergene alteration and weathering on the morphology and the chemical composition of antigorite, a non-regulated serpentine that shares chemical composition with asbestos chrysotile. Antigorite naturally occurring in lateritic Ni ores of New Caledonia exhibits a unique asbestos-like habit at the microscopic scale. Standardized mechanical stress was performed on antigorites, selected to represent different cohesion states. The specimens produced a relevant amount of respirable fibres, between 32 and 42% (WHO counting criteria). PCA on chemical data and ternary diagrams show that all antigorites exhibit a similar Si content (from 2.05 to 2.09 a.f.u.) but were mainly differentiated by Mg and Ni content, ranging from 2.66 to 2.80 and 0.00 to 0.09 a.f.u., respectively. Si content in Caledonian antigorite is higher than Si in non-lateritic samples. This suggests that a main alteration process occurred after the obduction of the ultramafic protolith. The supergene alteration determined the Ni enrichment of lateritic deposits and is likely the main cause of the mineral alteration of antigorite under sub-tropical environments. Further, weathering processes prompt the disaggregation of altered antigorite causing the generation and dispersion of respirable, potentially hazardous, antigorite fibres in the environment.

* Corresponding author at: Department of Chemistry, University of Torino, Via Pietro Giuria 7, I-10125 Torino, Italy.
E-mail addresses: jasminerita.petriglieri@unito.it, jasmine.petriglieri@gmail.com (J.R. Petriglieri).

https://doi.org/10.1016/j.scitotenv.2021.146185

1. Introduction

Inhalation is the most critical route of exposure to mineral fibres that becomes a matter of concern also in the case of exposure to Natural Occurrences of Asbestos (NOA) (Case et al., 2011; IARC, 2012). From a regulatory point of view, the term "asbestos" indicates six fibrous members of the amphibole and serpentine group of minerals. Following the pandemic exposure to asbestos during the last century, the six minerals are now classified as carcinogenic to human by International Agency for Research on Cancer (IARC)/World Health Organization (WHO) and banned or strictly regulated by safety and health protection organizations (e.g., NIOSH, OSHA, and EU). However, ban and regulations may not be applied to natural geological settings, where weathering events (e.g., erosion, landslide) and/or anthropic activities (e.g., agriculture, road grading, construction, mining; Gunter, 2018; Lee et al., 2008; Turci et al., 2016) may mobilize fibres from NOA-rich outcrops. The physical and biological alteration of exposed NOA-bearing outcrops prompts rock fragments to disaggregate, and this process may in turn generate inhalable elongated mineral particles (EMPs; NIOSH, 2011 definition). EMPs that share with asbestos many physico-chemical and toxicological properties may as well pose a risk to human health (Boffetta et al., 2018; Garabrant and Pastula, 2018; Harper, 2008; NIOSH, 2011). Few decades ago, an epidemic of malignant mesothelioma in three villages (Sarihidir, Tuzköy, and Karain) in the Cappadocia region in Turkey, was linked to the occurrence and use of deposits of fibrous erionite (Artvinli and Bariş, 1979). The carcinogenic potency of this naturally occurring fibrous zeolite is higher than crocidolite asbestos (Carbone et al., 2011; IARC, 2012). Asbestos-related mesotheliomas were also linked to the exposure to non-asbestos amphiboles winchite, richterite (EPA, 2014; Sullivan, 2007; Rogers, 2018), and fluoro-edenite (Gianfagna et al., 2003; IARC, 2017). To take into account this emerging group of potentially hazardous minerals, the U.S. EPA extended the term "asbestos" to the mixture of fibrous amphiboles (tremolite, winchite, richterite, etc.) identified in NOA-rich rocks found in vermiculite mine in Libby, Montana, U.S., where a cluster of asbestos-induced mesothelioma was observed (EPA, 2014; Meeker et al., 2003). In this context, several studies are trying to correlate bulk and surface properties of non-regulated EMPs with their potential toxicity. These studies included investigation on fibrous glaucophane, a sodic amphibole similar to crocidolite (Di Giuseppe et al., 2019; Erskine and Bailey, 2018), ferrierite, a sub-group of zeolite minerals (Gualtieri et al., 2018a), and antigorite, a member of serpentine family, chemically similar to chrysotile (Campopiano et al., 2018).

The risk associated to natural occurrences of asbestos and potentially hazardous EMPs should be adequately managed during activities that may release fibres in workplaces and in the environment. Quarrying and ore exploitation in EMP-bearing geological settings (e.g., serpentinites, albitites; Cavallo and Petriglieri, 2020; Gualtieri et al., 2014, 2018b; Vignaroli et al., 2013) need specific measures to protect worker health and the environment. Human activities and natural weathering, may, often synergistically, generate a large amount of airborne and waterborne EMPs and contaminate soils (Koumantakis et al., 2009; Turci et al., 2016; Fig. 1). A higher risk may result from the proximity to the mining site. An increase in the amount of lung-retained fibres, in humans or sentinel animals, has been directly linked to the time lived in the area, inversely linked to distance from mines, and correlated to a higher incidence of asbestos-related diseases among inhabitants (Campopiano et al., 2020; Case et al., 2002, 2011; Fornero et al., 2009; Ingravalle et al., 2020).

In the assessment of risk due to exposure to EMPs in mining context, nickel-ore exploitation from lateritic deposits is an outstanding site of investigation. Nickel laterite ores account for nearly 60% of the world's nickel production, and they remain the major source of Ni in the foreseeable future (Berger et al., 2011; Butt and Cluzel, 2013; Marsh et al., 2013). Nickel laterite ores are the product of supergene alteration of ultramafic rocks under humid sub-tropical conditions, providing to be a good case study for the investigation of the impact of EMP-disturbing agents, including both weathering and anthropic activities, on the formation and suspension of EMPs into the environment (air, water, soil, and waste; Fig. 1).

New Caledonia is one of the largest world producers of nickel from lateritic ores (McRae, 2020). The Caledonian ophiolite complex extends for more than a third of the land and consists of partially to totally serpentinized peridotites (Cluzel et al., 2001; Collot et al., 1987). Supergene alteration of the large ultramafic peridotites, associated with minor tectonic events, started the development of regolith that led to the present geomorphology and to the development of supergene nickel ores (Chevillotte et al., 2006; Cluzel et al., 2012; Cluzel and Vigier, 2008). Ore exploitation includes, besides nickel, the natural occurrence of fibrous serpentines, chrysotile and fibrous antigorite, and minor tremolite-actinolite asbestos (DIMENC-SGNC, 2010; Lahondère, 2007, 2012). When exposed to tropical climate conditions, EMP-deposits may be subjected to an additional process of alteration (e.g., erosion, leaching). As a result, mineral fibres occur in many different structures and morphologies ranging from blocky-prismatic crystals to flexible fibre bundles and individual fibres (Lahondère, 2007, 2012; Petriglieri et al., 2020b).

An increased incidence of asbestos-related diseases was highlighted in some areas of the island (Baumann et al., 2011; Goldberg et al., 1991). Baumann et al., 2011 evidenced an epidemiological correlation between mesothelioma incidence in residents and environmental exposure to fibrous serpentines, mainly fibrous antigorite and chrysotile. The great distribution over a large part of the island makes fibrous antigorite a potential public health issue. For these reasons, the government of New Caledonia included antigorite in the list of the regulated asbestos, applying the precautionary principle (Déliberation N°82 du 25 Aôut 2010). Nevertheless, the decree No 82/2010 does not discriminate between lamellar antigorite and fibrous antigorite and does not suggest a dedicated protocol for the risk evaluation and management of NOA-content.

Although correlation between the fibrous habit of chrysotile and its carcinogenic potency is universally accepted (IARC, 2012), a clear consensus on the definition of fibrous habit for antigorite has not been reached yet, and its potential toxicity is still under debate (ANSES, 2014). Additionally, the closely intergrowth of antigorite with other asbestos minerals also at the sub-millimetre scale often hinders the discrimination between antigorite and chrysotile (Dogan and Emri, 2000; Groppo and Compagnoni, 2007; Rooney et al., 2018). In the past, fibrous antigorite from a small asbestos mine near Rowland Flat, at northeast of Adelaide, in the South of Australia, was commercially exploited as asbestos (i.e., chrysotile). Only in recent years, during the remediation of the abandoned mine site, mineralogical studies identified the exploited asbestos as fibrous antigorite (Fitz Gerald et al., 2010; Keeling et al., 2008). To the best of our knowledge, this is the only case in which antigorite exhibiting an asbestos-like morphology was exploited and erroneously commercialized as chrysotile asbestos. Currently, there is a limited number of *in vitro* and *in vivo* toxicological investigations performed on lamellar and fibrous antigorite and the results of the studies are not conclusive (ANSES, 2014, and therein).

To foster the comprehension of the potential health hazard associated with the natural occurrence of antigorite in workplaces and in the environment, the physico-chemical properties related to the potential toxicity of antigorite must be investigated. The evaluation of fibre morphology and chemical composition are considered universally to be pivotal parameters in the comprehension of bulk structure relevant to toxicology. This work aims to define univocally the fibrous habit of Caledonian antigorite from macro- to microscale, and to provide the first description of its mineral chemistry. The work discusses the impact of supergene alteration and weathering on the morphology and chemical composition of antigorite from Ni-rich lateritic deposits.

A complete set of differently altered natural occurring antigorite samples coming from the Ni-open pits of New Caledonia has been selected. The fibrous habit of antigorite was firstly evaluated by optical

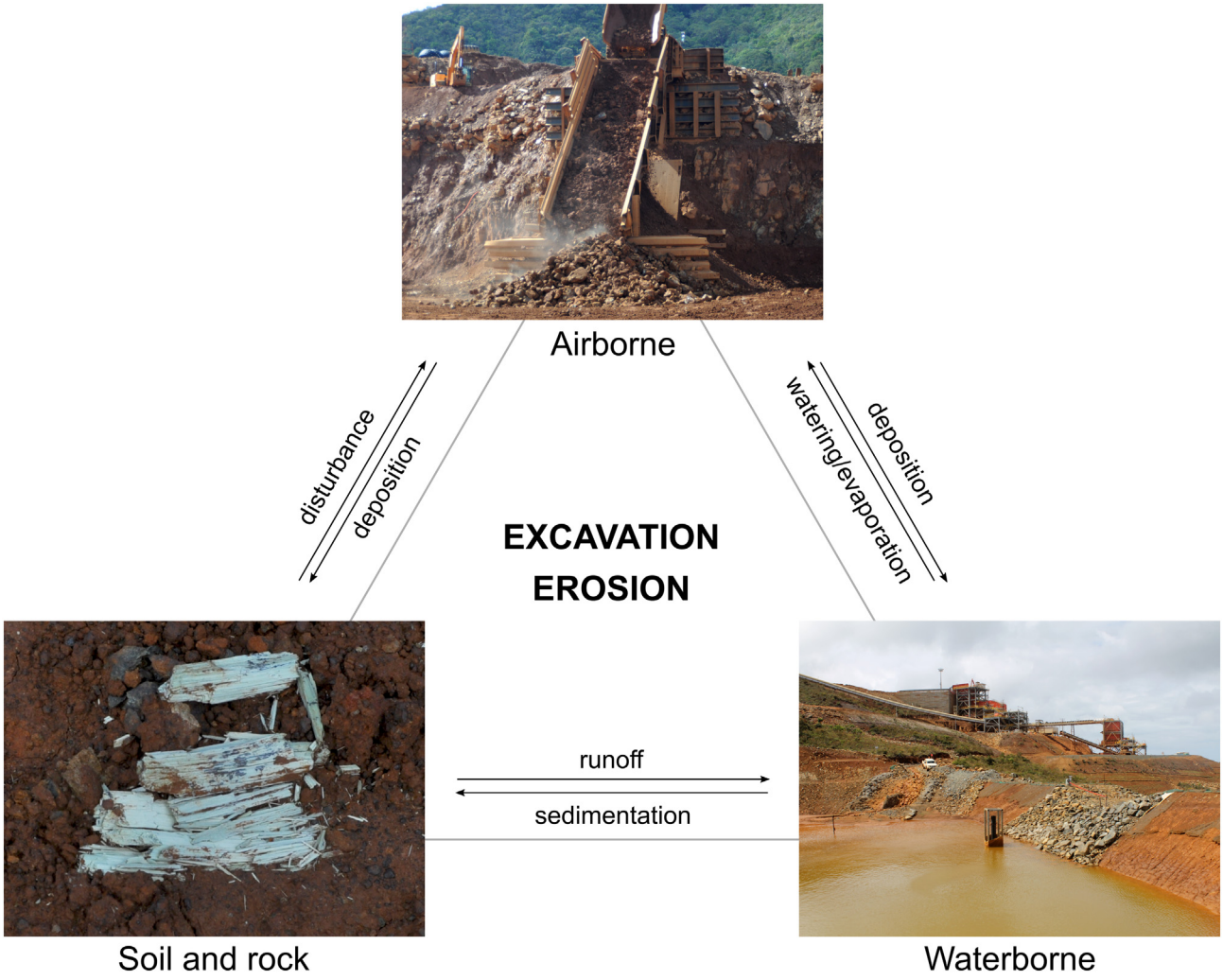

Fig. 1. Scheme illustrating the EMP pathways from NOA sources during Ni-ore exploitation activity.

and electron microscopy investigations. A petrographic optical observation associated with micro-Raman spectroscopy was carried out to discriminate the serpentine mineral phases and to characterize the mineralogical associations. X-Ray Powder Diffraction analysis was used to evaluate the presence of secondary mineral phases. The chemical composition of antigorite samples was comparatively investigated with Energy Dispersive X-Ray Spectroscopy (SEM-EDS). A statistical approach, consisting of Principal Component Analysis (PCA) and cluster analysis (k-means clustering), was adopted in supporting data interpretation.

2. Methods

2.1. Geological background

The Ni-laterite deposits of New Caledonia formed during the Neogene by lateritic alteration of obducted peridotite allochthonous unit, in which both residual and absolute economic nickel concentration has resulted from supergene enrichment (Troly et al., 1979). As shown in Fig. 2a, the peridotite allochthonous unit is composed of a main massif (Massif du Sud) located in the southernmost part of the island, and several tectonic klippes along the west coast (e.g., Koniambo Massif), covering more than one third of the island surface. The allochthonous unit, a portion of a supra-subduction oceanic mantle lithosphere, is formed of partially to totally hydrated harzburgite (>80%), dunite and minor lherzolite (in northern massifs only; Marchesi et al., 2009; Pirard et al., 2013). The degree of serpentinization may range from 20 to 60 vol%, and a more extensive serpentinization occurs at the basal layer of the regolith (Lagabrielle et al., 2013; Orloff and Gonord, 1968), where amphibole lenses may locally occur (Cluzel et al., 2012).

Ni-laterites formation started with the emplacement and serpentinization of the ultramafic protolith (Collot et al., 1987), followed by exposure to a humid sub-tropical climate and the development of a deep intensely weathered regolith (Chardon and Chevillotte, 2006; Fritsch et al., 2017). Lateritic Ni-ores formed by eluviation of nickel from the uppermost lateritic residuum and concentration in underlying saprolitic illuvium, by substituting Ni for Mg in secondary hydrous silicates (which can contain up to 5 wt% Ni) and in neoformed silicate, the garnierite minerals, which can grade over 20 wt% Ni (Butt and Cluzel, 2013; Pelletier, 1996). Subsequently, these deposits were subjected to further tectonic events (Chardon and Chevillotte, 2006; Chevillotte et al., 2006), which resulted in the current morphology (Fig. 2a). Owing to the high relief and the high erosion rate, the thickness of regolith in New Caledonia rarely reaches 40 m; silicate ores are 10–15 m thick. Where preserved, the upper part of the profile consists mainly of iron crust (Fig. 2b; Fritsch et al., 2017; Wells et al., 2009).

Fibrous varieties of serpentine minerals, mainly antigorite and chrysotile, combined with minor amount of tremolite-actinolite amphibole, are widespread in the saprolith horizon, currently mined in New Caledonia (Fig. 2b; Lahondère, 2007, 2012; Trotet, 2012). They generally outcrop along tectonic structural discontinuities as fractures, faults and shear zones (Lahondère, 2012). Lamellar to fibrous

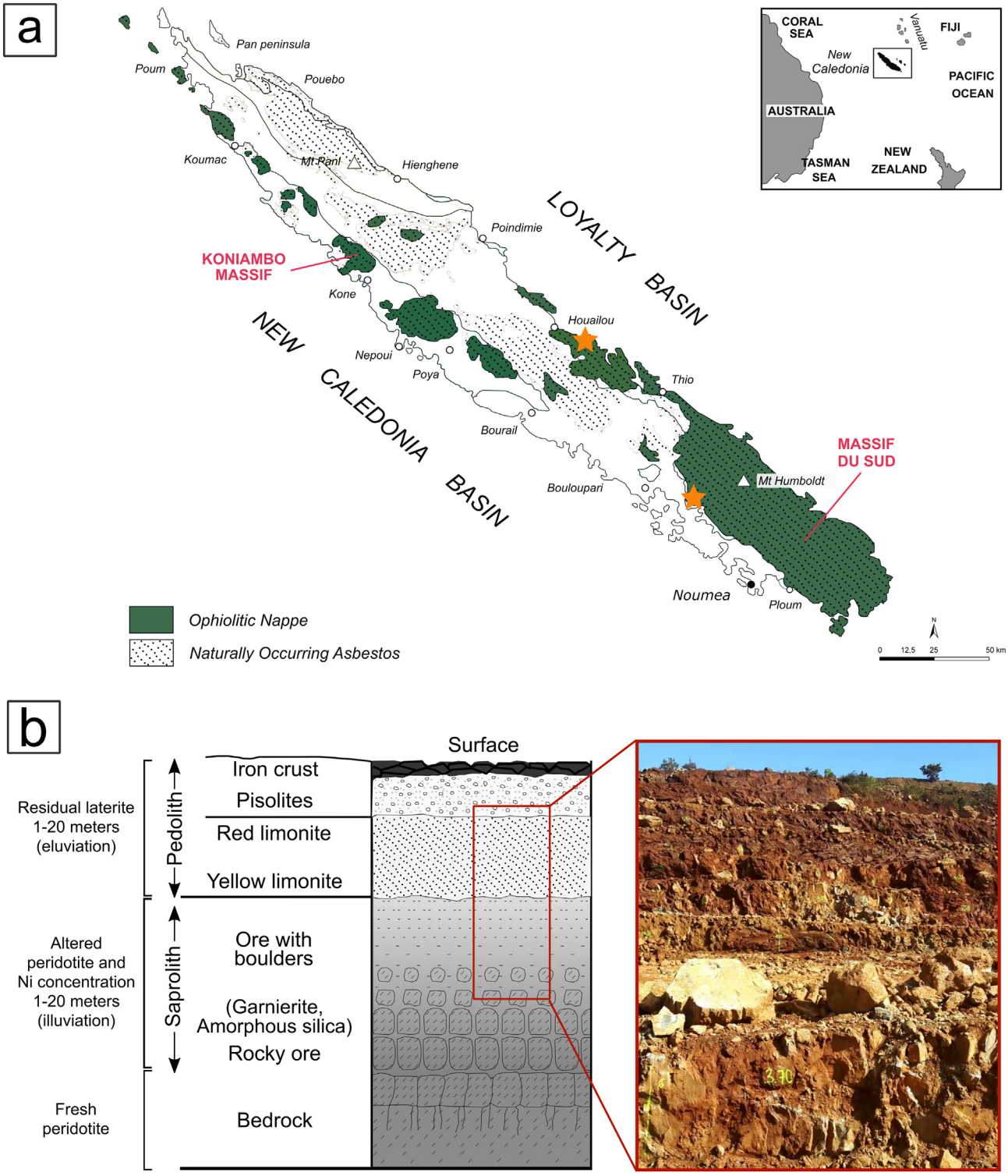

Fig. 2. a) Geological sketch map of the ultramafic allochthon unit of New Caledonia (redrawn and modified after Cluzel et al., 2001). Potentially NOA occurrences are reported (DIMENC-SGNC, 2010). Sampling sites of Tontouta (south-western coast) and Kouaoua (south-eastern coast) mines are indicated with star. b) Descriptive profile of a typical regolith of Ni-ore deposits with a zoom of the exploitation front site (modified after Robb, 2010). From the bottom to the top of the regolith the various horizons are bedrock (serpentinized peridotites), saprolith (rocky ore and earthy ore), soft yellow limonite (a clay soil rich in Fe-oxide), red limonite (a clay soil containing small grains of Fe-oxide) and finally the iron crust. (For interpretation of the references to colour in this figure legend, the reader is referred to the web version of this article.)

antigorite in serpentinized peridotites occur mainly as fracture-fill veins, closely related to the main faulting pattern. At the base of lateritic profile, antigorite exhibits a blocky-lamellar structure, from centimetres to decimetre. Moving up in the regolith profile, close to pedolith horizons, these planes become more fragmented and associated with fibres that seem to be originated from the extreme cleavage (fraying) of these same lath-shaped crystals. Veins and veinlets from centimetre to millimetre of chrysotile may also occur (Lahondère, 2007, 2012; Quesnel, 2015; Quesnel et al., 2016; Ulrich et al., 2010).

2.2. Sampling strategy

This work is part of a health risk assessment program, devoted to evaluate the professional exposure to asbestos and asbestos-like mineral fibres in NOA-rich mining sites of New Caledonia (for further details CNRT - Laporte-Magoni et al., 2018).

Field sampling was realized by professional geologist of mining companies. Sampling aims to collect a full set of antigorite specimens, representative of all types of antigorite occurrences encountered during the exploitation activity. A set of ten rock fragments collected from outcrops, tracks, and pits of mining sites of Tontouta (T, south-western coast) and Kouaoua (K, south-eastern coast) was selected for this work. A chrysotile specimen, fully described in previous work (sample S33, Petriglieri et al., 2020a), was added for comparison. Specific information on the provenance of rock fragments cannot be disclosed because they are subjected to confidential clauses. The summary of the characteristics of antigorite samples, including provenance, macroscopic structure, textural microstructure, and morphology is reported in Supporting Materials S1.

2.3. Methods

2.3.1. Scanning electron microscopy

Morphological investigation was carried out on natural samples with a Scanning Electron Microscope (SEM) JEOL JSM-IT 300 LV/LA with Low Vacuum Mode equipped with an Oxford-X-Max EDS. Secondary Electron Images (SEI) were acquired at various magnifications and accelerating voltages, commonly 3–10 kV.

2.3.2. Flow particle image analysis

Particle shape and particle size distribution of powdered antigorite in a range of 0.8–300 μm were obtained by Flow Particle Image Analysis (FPIA) using the Sysmex FPIA-3000 apparatus (Malvern Instruments).

Three antigorite samples (T1, T3, and T7) were ground in a ball mixer mill (Retsch MM200, Haan, Germany) for 2 min (27 Hz). Agate jars were used to avoid metal contamination. After grinding, antigorite powders were dispersed in ultrapure water (0.5 mg/ml) and sonicated for 30 s at 10 W. Each suspension was passed through a cell where images of particles were captured using stroboscopic illumination and a CCD camera (20× magnification lens).

2.3.3. X-ray powdered diffraction

XRPD patterns were collected using an X-Ray wide angle diffractometer INEL CPS 120. Operating conditions were 30 kV and 30 mA. The transmitted X-ray beam is produced from a filtered Co source Kα1 ($\lambda = 0.178897$ nm). The intensity of the diffracted beam is recorded with a curved position-sensitive detector between 0° and 120° (2θ) at a step size of 0.03°. Resolution width varies slightly from 0.10° to 0.15° in 2θ (from small angles to large angles). X-Ray diffraction patterns were acquired at all angles simultaneously.

Powder samples were prepared by gentle hand grinding in an agate mortar. All data interpretations were performed with the Match! Software.

2.3.4. Micro-Raman

Raman spectra were obtained with a Horiba JobinYvon HR800 Raman spectrometer equipped with an Olympus BX41 confocal microscope, a 600-grooves/mm holographic grating monochromator and a high-gain Peltier-cooled CCD. A Nd solid state laser at 532-nm has been used as excitation and neutral density filters were used to avoid sample heating. Spectra were obtained on petrographic thin sections with a 100× objective. Under these working conditions, the minimum lateral resolution is around 2 μm and the resolution along z-axis is ca. 1 μm. The spectrometer was calibrated using the 520.7 cm^{-1} Raman peak of silicon before each experimental session. Spectra were collected as follows: 15 acquisitions for 10 s in the low and high wavenumber spectral range were averaged and background subtracted with LabSpec® software.

2.3.5. Chemical analysis

Chemical analysis was performed on petrographic thin sections with a Scanning Electron Microscope associated to Energy dispersive X-ray spectroscopy (SEM-EDS) JEOL JSM IT 300 LV equipped with an Oxford INCA Energy 200 ED. An automated approach descripted in Supporting Materials (Supporting Materials 5a and b) was adopted to collect a representative, statistically significant number of EDS point analyses on elongated (fibrous) crystals of antigorite occurring with several textures. Microanalysis operating conditions were 15 kV and 5 nA, 10^5 CPS and 30 s counting time; relative wt% errors are <1% for major elements and <5% for minor components. Standards comprise pure elements, oxides and/or silicate. Before the analysis, samples were coated with a carbon layer.

The EDS chemical data were analysed by means of a statistical approach, consisting of multivariate analysis (cluster analysis and Principal Component Analysis). Statistical data treatment was performed with OriginPro® software.

3. Results

At the hand scale, antigorite fragments exhibited an appearance from massive (T1, T2) to powder-disintegrated (T7, T8), and are coloured from pale-green (T1, T2, K2) to white (T3, T6, T8), as shown in Fig. 3. Samples T1 and T2 were cohesive, dominated by platy-shaped fabric of welded and parallel blades. Samples K1, K2, and T3 showed a weak cohesion and a more friable aspect, dominated by fragments cracking with poor cleavage into thin curvilinear laminas. Samples T4, T5, T6, T7, and T8 showed an extremely weak cohesion, consisting of a powder-disintegrated material, where fibro-lamellar blades occur randomly orientated to form aggregates and bundles. The three descriptive categories were exemplified in Fig. 4 using three representative antigorite samples to highlight the different degree of cohesion.

The morphological investigation of antigorite samples under optical and electron microscopies was firstly conducted on fragments non-subjected to any preparation and/or mechanical stress (e.g., crushing, grinding). At the microscopic scale, all specimens were fibrous in nature. As displayed in Fig. 3, SEM images revealed the fibrous nature of antigorite samples, which consist of poly-filamentous bundles of tightly packed fibres and fibro-lamellae. Antigorite elongated particles appear flexible and longitudinally separated into thinner fibres. Bundles of parallel elongated lath-shaped crystals present regular (e.g., T8) or irregular endings (e.g., T6), with splayed or frayed ends. Aggregates of randomly oriented non-elongated blades may also occur (T4). However, most of crystals maintain their elongated shape displaying a gradual fibrous ending, which appear bent, slinky to curvilinear (Supporting Materials S2).

To estimate the potential risk associated with antigorite types from New Caledonia outcrops, the fibrous habit and size distribution of antigorite particles and fibres after a standardized mechanical stress were estimated by means of light microscopy coupled with automated image analysis (FPIA) (Fig. 5). Samples were gently crushed in a ball mixer mill for 2 min at 27 Hz in agate jars. After milling, all antigorite samples preserved their fibrous morphology indicating that antigorite fractures easily along z-axis. Standardized milling generated around 50% of elongated, fibrous particles, most of which have the dimensional characteristics of respirable fibres ($L > 5$ μm, $D < 3$ μm, $L/D > 3$), according to the dimensional criteria proposed by WHO for toxic mineral fibres (IARC, 2012; WHO, 1997). The number of respirable fibres represents up to 42% of the total particles and does not appear to be correlated with the cohesive state of the samples at the field scale (Fig. 2).

The bulk rock mineralogical composition of samples (XRPD analysis, Supporting Materials S3) mainly consists of serpentine, with a limited

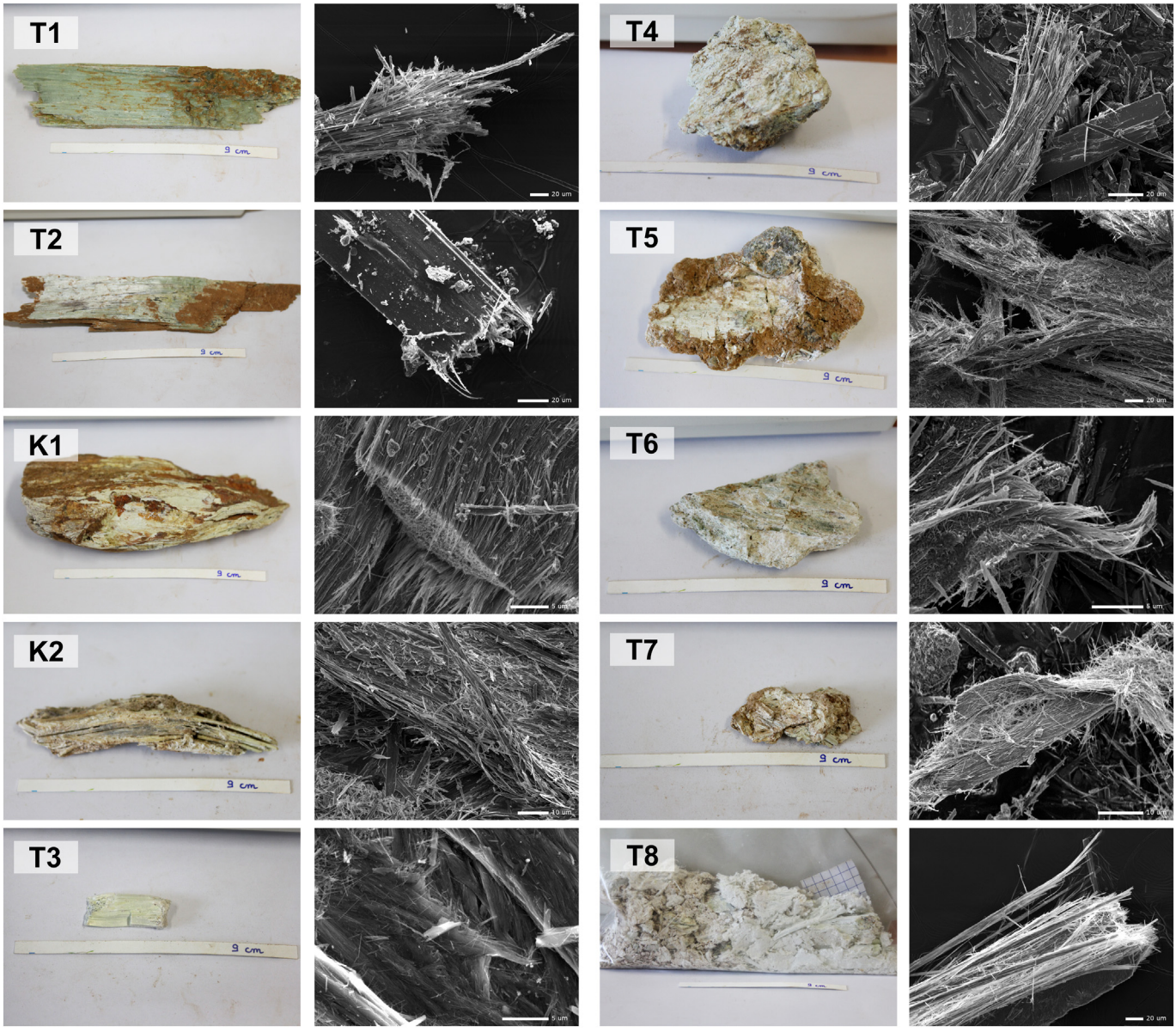

Fig. 3. Morphological characterisation. Hand specimens (on the left) and representative SEI images (on the right) of antigorite samples arranged in decreasing order of macroscopic cohesion, from massive to powder-disintegrated appearance. Despite the macroscopic structure, all samples show a fibrous habit at microscopic scale.

amount of Fe-oxide magnetite (samples T1, T4, T5) or quartz (samples K1, T8).

Light microscopy petrographic observation of thin sections enhanced by *in situ* Raman analysis allowed describing the association of the mineral phases of each sample (Fig. 6 and Supporting materials S4). Generally, the petrographic description of the main textures of serpentine structures relies on the classification of Wicks and Whittaker, 1977 (e.g., Andreani et al., 2007; Mothersole et al., 2017; Ribeiro Da

Fig. 4. Macroscopic description of the three cohesive state of antigorite specimen from nickel ores. The representative images describe the different cohesion of natural occurring antigorite samples, from massive to moderately to weakly cohesive (T1, T3, and T7, respectively).

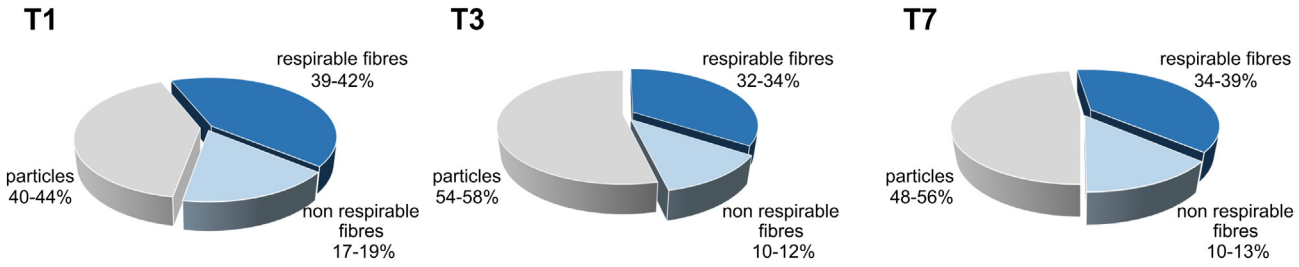

Fig. 5. Antigorite particle size distribution after gentle mechanical grinding detected by optical microscopy and automated image analysis. Pie charts show the % of particles with L/D > 3 (EMPs, according to NIOSH definition, ANSES, 2017; NIOSH, 2011) and WHO fibres (L/D > 3, D < 3 μm, L > 5 μm; WHO, 1997).

Costa et al., 2008). Antigorite is typically recognized for its interpenetrating or interlocking texture. These textures should be observed in any direction non-parallel to the preferential orientation of the lath-shaped crystals (mineral lineation). Under the optical microscope, antigorite appeared colourless to pale green and had fine to very fine grain size (Supporting Materials S4). Only in some specimens, antigorite

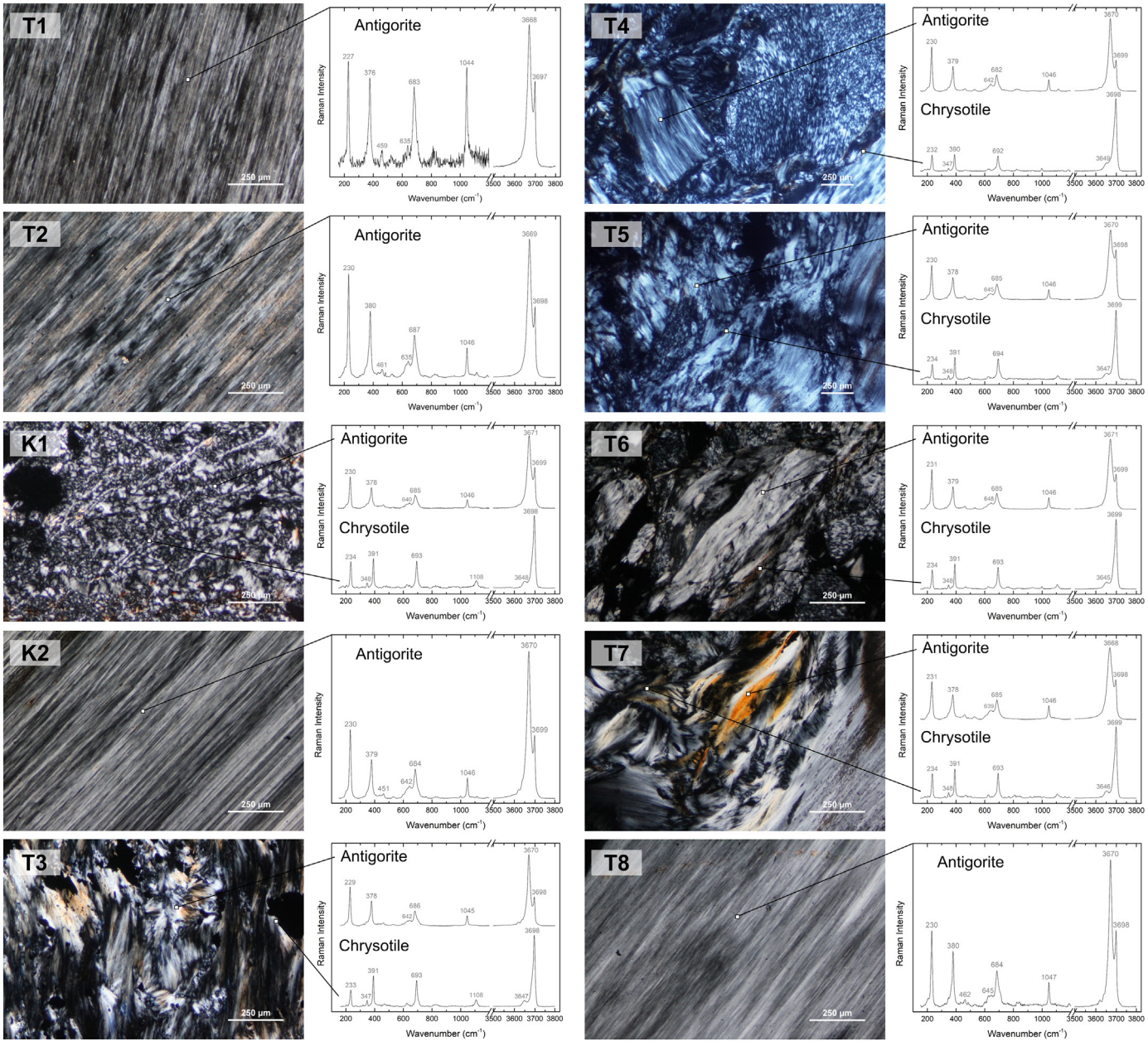

Fig. 6. Textural description and serpentine phase identification. Representative optical photomicrographs showing characteristic textures of antigorite samples (cross-polarized light), associated with relative micro-Raman analyses. Raman spectra were obtained at 532-nm in the extended region.

occurred as fragments from medium to large grain size (T4, T5, T6, and T7). Opaque minerals, mainly magnetite, occurred as very fine elongated crystals, locally arranged in isooriented alignments between adjacent fibres or at the vein salvages. Rarely, they exhibited a dendritic structure and/or a larger grain size. The samples generally showed a complex microstructure matrix, consisting of the coexistence of several textures. Antigorite showing a preferential elongation direction is formed by parallel streaks of elongate and fibrous crystals (T1, T2, K2, and T8). The fibrous shape was especially evident under crossed polarizers due to the small differences in the extinction positions, which tend to be straight, and colours of interference of adjacent and parallel fibres. Antigorite consisting of randomly orientated aggregates showed more types of shapes and intergrowths. Antigorite occurred mainly with the typical interpenetrating and/or interlocking microstructure (T3, T4, T5, and T6). Small elongate crystals may display a sub-parallel arrangement (K1). Later cross- and slip-type veins of antigorite, and minor chrysotile, may develop on the interpenetrating matrix (T4), displaying sometimes a banded microstructure (T5). Very fine antigorite may grow with a fibrous-radiated structure, elongate crystals are arranged to form a star- and fan-like texture of divergent, often branching fibres (T3, T7).

A minor contamination by chrysotile was often observed, due to the typical closely intergrowth of these serpentine minerals in metamorphic context (Dogan and Emri, 2000; Groppo and Compagnoni, 2007; Tarling et al., 2018). Even though optical polarizing microscope might lead to misassign fibrous antigorite and chrysotile veins, the use of micro-Raman spectroscopy to discriminate among serpentine minerals confirmed that antigorite is the dominant serpentine phase of all samples investigated. The presence of the typical doublet in the OH-stretching region, with the main peaks located at about 3665 and 3695 cm^{-1}, allowed to confidently assign antigorite (Auzende et al., 2004; Groppo et al., 2006; Petriglieri et al., 2015; Rinaudo et al., 2003). Chrysotile, in the form of sub-micrometric isotropic veinlets and/or brownish cemented veins, was occasionally observed (samples K1, T3, T5, T6, T7) mainly in the grain boundaries and cleavage between antigorite crystals (Fig. 6) and discriminated from antigorite due to the main OH-stretching vibration at 3698 cm^{-1} (Petriglieri et al., 2015; Tarling et al., 2018).

To explore the chemical variability of the antigorite samples under investigation, a study of variability in elemental chemical composition of the antigorite phases in each sample was carried out with a two-step approach: i) an explorative statistical tool, consisting of Principal Component Analysis (PCA) associated with k-means clustering analysis, was used to group samples into homogeneous classes of similar chemical composition; ii) a main elemental compositional clustering was therefore applied to these sub-group to obtain ternary diagrams. For each sample, about 300 EDS point analyses on elongated fibrous crystals were collected on petrographic thin section (Supporting materials S5a). Representative microanalyses for each sample are reported in Table 1.

PCA analysis reduced the variance of the eleven major elements (Si, Al, Cr, Fe, Ni, Co, Mg, Mn, K, Na, and Ca) to a minimum number of principal components, which describe more than 90% of the variance of the analyses. In our dataset, the three principal components described the 97.46% of the total variance of the system, the two-dimensional graph obtained plotting principal component PC1 vs. PC2, and PC2 vs. PC3 are reported in Fig. 7. The eigenvectors (blue lines) localise the contribution given by single elements, whereas the eigenvalues (the vector magnitude) are related to covariance of the dataset in that variable. In the plot PC1 vs. PC2 (Fig. 7a) samples showed a greater variability along three principal eigenvectors, the Mg, Ni, and Fe—Si directions, arranging the dataset of the EDS analyses in three main populations. The plot PC2 vs. PC3 (Fig. 7b) evidenced a difference in elemental composition for samples K1 and K2, showing a Fe-rich and Si-rich content, respectively. K-means clustering analysis confirmed that the number of clusters present in the dataset is three (for further details see Supporting Materials S6).

On the basis of PCA results, EDS data were plotted on ternary diagrams, considering Si, Mg, Ni and Fe elements, as shown in Fig. 8.

Triangular diagrams considering Si-(Mg + Fe)-Ni (Fig. 8a) and Si-(Mg + Ni)-Fe (Fig. 8b) are commonly used to describe the chemical weathering of Mg/Ni phyllosilicates (garnierite) from lateritic Ni-ore deposits (e.g., Fritsch et al., 2014; Villanova-de-Benavent et al., 2014). All samples investigated are positioned in a more Si-rich area with respect to the stoichiometric serpentine considered as reference (black line in the diagrams). A significant depletion in Mg and an enrichment in Si content was observed. When plotted on a Si-(Mg + Fe)-Ni system

Table 1
Representative SEM-EDS analysis (in weight percent) and structural formulae (in atoms per formula unit) of antigorite samples. Chemical analyses were normalized on the basis of seven oxygen. The full set of EDS analyses is reported in Supporting Material S5b.

	Ctl	T1	T2	T3	T4	T5	T6	T7	T8	K1	K2
Analysis	12	287	103	487	910	66	559	108	914	2	3
SiO_2	44.24	43.87	44.16	44.19	42.60	42.71	43.31	44.13	44.40	44.67	43.87
Al_2O_3	0.24	0.59	0.17	0.19	0.27	0.24	0.35	0.23	0.17	0.00	0.27
Cr_2O_3	0.00	0.00	0.00	0.00	0.00	0.00	0.00	0.00	0.00	0.00	0.07
FeO	1.49	1.98	2.35	1.95	1.99	2.57	3.20	2.72	1.70	2.73	3.85
NiO	0.16	2.47	2.29	0.53	0.00	0.00	0.48	0.33	0.21	0.37	0.34
Co_3O_4	0.00	0.00	0.00	0.00	0.00	0.00	0.02	0.09	0.00	0.00	0.08
MgO	40.57	38.02	38.03	39.30	38.21	37.45	37.62	38.64	39.57	38.21	37.96
MnO	0.00	0.00	0.00	0.11	0.12	0.15	0.11	0.07	0.00	0.00	0.04
K_2O	0.05	0.00	0.00	0.00	0.00	0.00	0.02	0.04	0.00	0.00	0.01
NaO	0.17	0.13	0.11	0.15	0.12	0.16	0.15	0.16	0.16	0.12	0.13
CaO	0.14	0.07	0.00	0.00	0.00	0.00	0.01	0.06	0.06	0.00	0.04
Tot	87.06	87.13	87.11	86.42	83.31	83.28	85.27	86.47	86.27	86.10	86.66
Si	2.050	2.057	2.071	2.068	2.063	2.075	2.068	2.072	2.073	2.099	2.066
Al	0.013	0.033	0.010	0.011	0.016	0.014	0.019	0.013	0.010	0.000	0.016
Cr	0.000	0.000	0.000	0.000	0.000	0.000	0.000	0.000	0.000	0.000	0.002
Fe	0.057	0.078	0.092	0.076	0.081	0.105	0.128	0.107	0.067	0.107	0.152
Ni	0.006	0.093	0.086	0.020	0.000	0.000	0.019	0.012	0.008	0.014	0.013
Co	0.000	0.000	0.000	0.000	0.000	0.000	0.001	0.004	0.000	0.000	0.004
Mg	2.802	2.658	2.659	2.741	2.759	2.712	2.678	2.703	2.754	2.676	2.665
Mn	0.000	0.000	0.000	0.005	0.005	0.006	0.005	0.002	0.000	0.000	0.001
K	0.002	0.000	0.000	0.000	0.000	0.000	0.001	0.002	0.000	0.000	0.000
Na	0.014	0.012	0.011	0.013	0.011	0.014	0.014	0.014	0.014	0.011	0.012
Ca	0.007	0.004	0.000	0.000	0.000	0.000	0.000	0.004	0.002	0.000	0.002
Tot	4.95	4.93	4.93	4.93	4.93	4.93	4.93	4.93	4.93	4.91	4.93

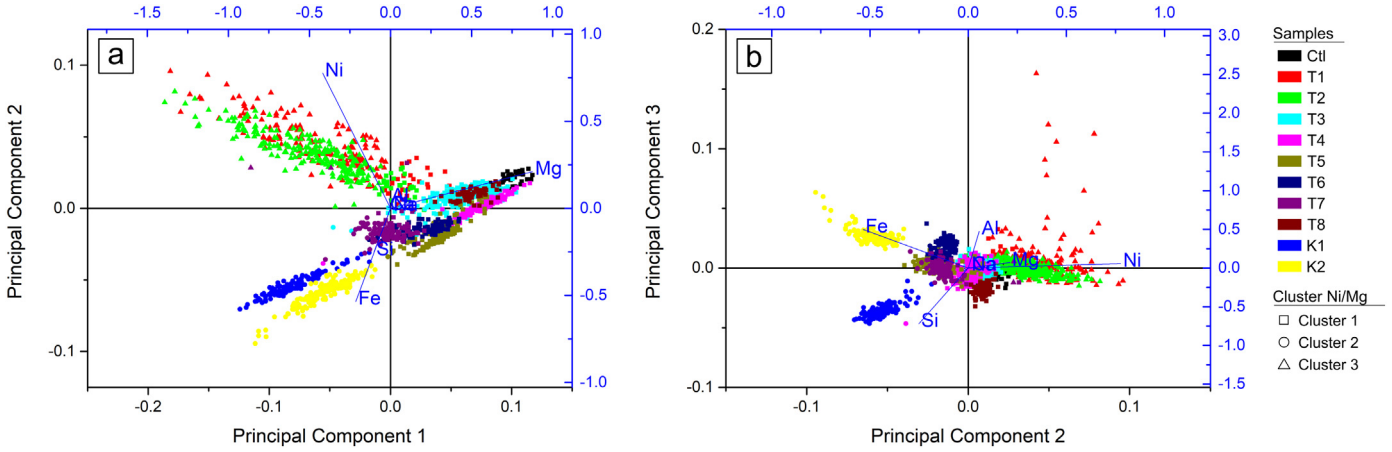

Fig. 7. PCA associated to k-means clustering analysis of EDS microanalysis of antigorite samples. Biplot of the EDS compositional data (a.f.u.). The vectors are the eigenvectors of the covariance matrix. K-means clustering relies on the stoichiometric ratios Ni—Mg. A sample of Caledonian chrysotile (Ctl) (Robb, 2010) is included for comparison.

(Fig. 8a), most samples displayed a consistent composition in Mg + Fe and Si, and only sample K1 exhibited a higher amount in Si. Samples T1 and T2 showed a low Mg + Fe content and a relative high Ni content. The plot Si-(Mg + Ni)-Fe (Fig. 8b) confirmed the higher amount in Si for sample K1 and showed a higher content in Fe for samples K1 and K2. Plotting Mg, Fe, and Ni elements (Fig. 8c) major differences in composition were observed. Samples spread along two main axes, the Mg—Fe and the Mg—Ni axes, clustering in the following populations: i) Mg-rich and Ni-poor (from T3 to T8), ii) Ni-rich and Mg-intermediate (T1, T2), and Fe-rich and Mg-poor (K1, K2).

4. Discussion

Morphology and crystal chemistry represent some of the most relevant parameters involved in the evaluation of the hazard of mineral fibres. Fibre morphology determines deposition, translocation, and clearance in the lung, ultimately driving the fibre fate following inhalation (Turci et al., 2017). If the six commercial asbestos fibres are well defined for their hazardous morphological parameters (IARC, 2012), natural non-asbestos mineral fibres may occur in a large number of complex and intermediate shapes (Belluso et al., 2017). Despite several studies refers to the common presence of fibrous antigorite in NOA context (e.g., Belluso et al., 2020), only a few examples of fibrous asbestos-like antigorite have been reported (Campopiano et al., 2018; Groppo and Compagnoni, 2007; Keeling et al., 2008). In fact, even when antigorite was claimed to be “asbestiform” or “asbestos-like”, the mineral showed an intermediate stage from a platy to a fibrous habit (e.g., Vortisch and Baur, 2018). More frequently authors, including some of us, tried to highlight the *quasi* asbestos-like habit of antigorite assessing its “pseudo-fibrous” form (Cavallo and Petriglieri, 2020; Cavallo and Rimoldi, 2013; Favero-Longo et al., 2013; Groppo and Compagnoni, 2007; Viti, 2010). This work suggests that antigorite samples from lateritic units of New Caledonia distinguish from the rest of the samples investigated so far, for their unique fibrous asbestos-like morphology. All samples collected and analysed in this work display an intermediate morphology between chrysotile and amphiboles asbestos. Antigorite from New Caledonia shares with chrysotile the polyfilamentous behaviour, consisting of the packing of very long and thin elongated particles, and shares with amphibole asbestos the quite rigid acicular and lath-shaped habit, commonly described for tremolite asbestos. Interestingly, the fibrous asbestos-like habit is strongly preserved (up to 42% of respirable fibres on total particles) when samples are subjected to mechanical stress (e.g., ball milling). This behaviour of Caledonian antigorite poses concern because mechanical operations involving rock disturbance might easily release airborne and waterborne elongated respirable particles that may pose a risk for human health and the environment. Conversely, the occurrences of pseudo-fibrous antigorite (e.g., Cavallo and Rimoldi, 2013) consists mainly of the packing of flexible elongated platy blades. In this latter case, the lamellar shape is predominant over the fibrous shape. So far, the Rowland Flat fibrous antigorite represents the occurrence with the closest morphology to the Caledonian antigorite (Rowland Flat area, Barossa Valley, South Australia; Fitz Gerald et al., 2010; Keeling et al., 2008) and the comparative evaluation of the chemical, morphological, and toxicological aspects is under investigation.

It is worth noting, that the macroscopic cohesion state of antigorite rock fragments often misguides professional geologists and researchers in the identification of fibrous antigorite. Indeed, the fibrous nature of Caledonian antigorite seems not to be whatsoever related to the macroscopic aspect of the hand sample that ranged from compact-massive to powder-disintegrated. Due to the lack of correspondence between macroscopic and microscopic morphology, the discrimination of the potentially hazardous asbestos-like EMPs from the non-hazardous particles during excavation activities in mining site or in not exploited natural outcrops is quite challenging. Hand samples characterized by a massive, lamellar, and cohesive aspect can be made by the closed overlapping of bundles and/or aggregates of fibres and fibro-lamellae. The fibrous nature of these samples is evident only increasing the scale of magnification.

The complexity recorded in rock fabrics (meso-scale), macroscopic structures (hand-scale), and textures (arrangement of crystals at the microscale) depends on the type of geological processes responsible for the mineral crystallization and on the type of weathering processes responsible for the mineral alteration. Differences in chemical composition keeping memory of the serpentinization processes (Frost et al., 2013 and references therein), and of the supergene alteration of rocks by evaluating the chemical depletion (or the enrichment) in peculiar major or trace elements.

The origin of fibrous antigorite occurrences was mainly related to synkinematic fibrous seals associated with the opening of tension cracks, or motion along micro-faults during obduction episode (Cluzel et al., 2020; Cluzel and Vigier, 2008). Cluzel et al., 2020 dated the crystallization of fibrous antigorite bearing-veins to a secondary serpentinization episode, related to the upward decreasing serpentinization of intra-oceanic serpentine fractures formed during cooling and hydration of mantle lithosphere. Post-obduction, supergene alteration, that is responsible for the formation of Ni-ore laterite, promoted the chemical alteration of antigorite fibres. Leaching processes, and consequently redistribution of the elements in the profile, led to a chemical variation especially in Mg and Ni. Fe-enrichment (e.g., Kouaoua samples K1 and K2) may be ascribed to intrinsic chemical variability of serpentine phases in lateritic

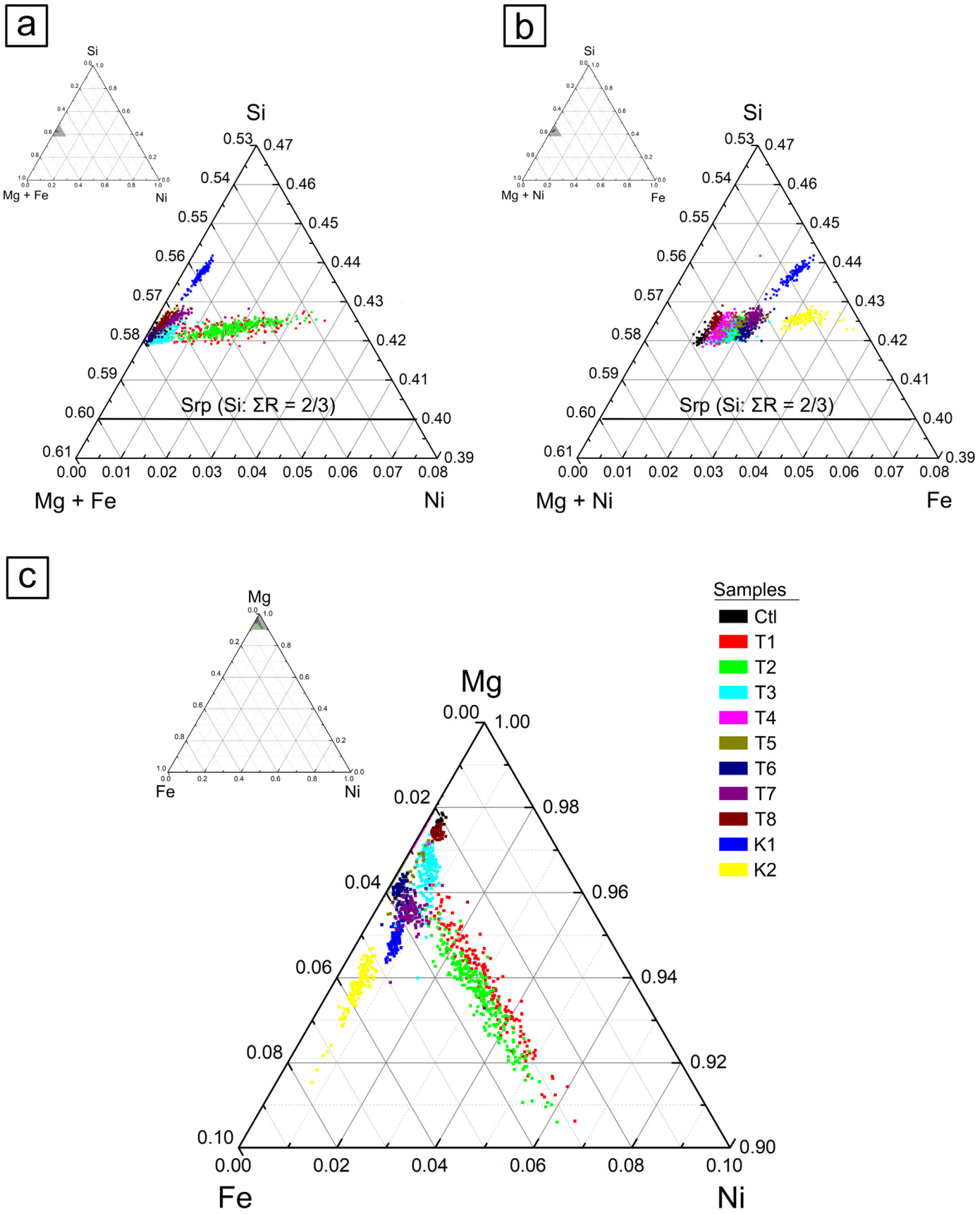

Fig. 8. Ternary diagrams (a) Si-(Mg + Fe)-Ni, (b) Si-(Mg + Ni)-Fe, and (c) Mg-Fe-Ni showing the variability in chemical composition of antigorite samples, plotted as atoms per formula unit. A sample of Caledonian chrysotile (Ctl) is included for comparison. Stoichiometric Mg and Ni end members of serpentine (Srp) are indicated for reference.

context, which confirmed to be generally not significant (Cavallo and Rimoldi, 2013) compared to natural variability within saprolitic horizon (Villanova-de-Benavent et al., 2014, 2016). The chemical evidence of a comparable amount of Si in all of the investigated samples (Fig. 8a and b) suggests that Caledonian antigorites are the results of a sequence of similar geological events, that starts with the ocean-floor metamorphism of the parent-rock, and concludes with the exposure of formed Ni-bearing serpentine veins to weathering. During these events, the partial or total transformation of the primary olivine and orthopyroxene minerals produces Ni-rich serpentine, talc, and smectite, without altering the mineral Si content. During the laterization process, indeed, any silica possibly released during the transformation of orthopyroxene is reabsorbed by the newly formed minerals.

Comparing Caledonian with non-lateritic antigorites (e.g., Groppo and Compagnoni, 2007), lateritic antigorites show a significant higher Si and a lower Mg content. This evidence the lower alteration of the non-lateritic antigorites and the strong chemical modification induced by supergene alteration. The main chemical differentiation is highlighted indeed by the antigorite distribution along the Mg—Ni axis (Fig. 8c), where the Ni—Mg cation exchange is observed. These minerals have a composition that varies from magnesian to nickeliferous endmembers. T1 and T2 antigorites show a higher Ni amount (about 2.4% wt. NiO) compared to the other antigorites, which exhibit a NiO content of ca. 0.3%wt. (Table 1). T1 and T2 are both characterized by a similar macroscopic structure that consists of a cohesive appearance, dominated by the close packing of welded and parallel fibrous elongated particles. Matching the NiO content of samples with the distribution of Ni ore in lateritic regolith profile of New Caledonia deposits (Fritsch et al., 2017), the occurrence of the most compact fragments in the upper part of the saprolitic horizon is consistent with the high Ni concentration produced by illuviation. The exploitation activity of this horizon provokes the exposition of antigorite-bearing to weather. Once exposed, these veins are subjected to heavy physical and biological weathering processes, which are probably the main agents causing mechanical disruption and disaggregation of altered antigorite. Such processes can release fibrous elongated particles into soil, air, and water. The circulation and percolation of meteoric water, flowing preferentially into cracks, fissures, and faults, often associated with the occurrence EMP veins, promote the disaggregation and dispersion of potentially hazardous antigorite fibres. The powdery appearance of some field samples can be ascribed to the weathering processes that impact rock disaggregation in subtropical area.

Moreover, following this multi-step process of alteration, a modification of surface chemical composition of these fibres is assumed. The characterisation of surface physico-chemical parameters that might modulate the hazard antigorite fibres from New Caledonia is outside the scope of this work and it will be the subject of a future paper.

5. Conclusion

The study of morphology and crystal chemistry is a pivotal first step in the investigation of the potential hazard of non-regulated elongated mineral particles (EMPs) in NOA-rich deposits. This work describes for the first time the fibrous, asbestos-like habit of Caledonian antigorite, providing a comprehensive illustration of the relationships among structure (hand-scale), textures (arrangement of crystals at the micro-scale), and morphologies of altered samples from Ni-rich lateritic deposits. Our data indicate that structural properties at the macroscopic scale are not extended at the microscopic scale, highlighting the peculiar asbestos-like habit for both massive and powdered-disintegrated antigorites. Comparison with antigorites from non-lateritic environment evidences the relevant chemical effect of supergene alteration on the antigorite chemistry. Furthermore, the mechanical disruption induced by weathering processes prompts the disaggregation of altered antigorites causing the generation and dispersion of respirable antigorite fibres in the environment (air, water, and soil). The identification of these EMPs at any scale of magnification is therefore strongly encouraged for a proper NOA risk assessment.

CRediT authorship contribution statement

Jasmine R. Petriglieri: Conceptualization, Methodology, Writing – original draft, Writing – review & editing. **Christine Laporte-Magoni:** Conceptualization, Supervision, Resources. **Emma Salvioli-Mariani:** Methodology, Supervision, Writing – review & editing. **Simona Ferrando:** Methodology. **Maura Tomatis:** Methodology. **Bice Fubini:** Project coordination. **Francesco Turci:** Conceptualization, Methodology, Writing – original draft, Writing – review & editing, Resources.

Declaration of competing interest

The authors declare that they have no known competing financial interests or personal relationships that could have appeared to influence the work reported in this paper.

Acknowledgments

This study is a part of a multidisciplinary project “Amiantes et Bonnes Pratiques (ABP)” supported by the Centre National de Recherche Technologique (CNRT- Nouvelle Calédonie).

JRP post-doc position is funded by the University of Torino (CHI.2019.08/XXI “Development of innovative tools for the risk assessment of elongated mineral particles (EMP) in natural environment”) and by the INAIL - BRIC 2019 project (grant number ID 57.1).

Micro-Raman spectra have been obtained with the equipment acquired by the Interdepartmental Centre “G. Scansetti” for Studies on Asbestos and Other Toxic Particulates with a grant from Compagnia di San Paolo, Torino, Italy.

The authors kindly acknowledge Dr. L. Barale for reviewing the manuscript.

Appendix A. Supplementary data

Supplementary data to this article can be found online at https://doi.org/10.1016/j.scitotenv.2021.146185.

References

Andreani, M., Mével, C., Boullier, A.M., Escartín, J., 2007. Dynamic control on serpentine crystallization in veins: constraints on hydration processes in oceanic peridotites. Geochemistry, Geophys. Geosystems 8, 1–57. https://doi.org/10.1029/2006GC001373.

ANSES, 2014. Évaluation de la toxicité de l’antigorite. Maisons-Alfort, France.

ANSES, 2017. Particules minérales allongées. Identification des sources d’émission et proposition de protocoles de caractérisation et de mesures, Maisons-Alfort, France.

Artvinli, M., Bariş, Y.İ., 1979. Malignant mesotheliomas in a small village in the Anatolian region of Turkey: an epidemiologic study. J. Natl. Cancer Inst. 63, 17–22.

Auzende, A.L., Daniel, I., Reynard, B., Lemaire, C., Guyot, F., 2004. High-pressure behaviour of serpentine minerals: a Raman spectroscopic study. Phys. Chem. Miner. 31, 269–277. https://doi.org/10.1007/s00269-004-0384-0.

Baumann, F., Maurizot, P., Mangeas, M., Ambrosi, J.-P., Douwes, J., Robineau, B.P., 2011. Pleural mesothelioma in New Caledonia: associations with environmental risk factors. Environ. Health Perspect. 119, 695–700. https://doi.org/10.1289/ehp.1002862.

Belluso, E., Cavallo, A., Halterman, D., 2017. Crystal habit of mineral fibres. In: Gualtieri, A.F. (Ed.), Mineral Fibres: Crystal Chemistry, Chemical Physical Properties. Biological Interaction and Toxicity. European Mineralogical Union and the Mineralogical Society of Great Britain & Ireland, UK, pp. 65–109 https://doi.org/10.1180/EMU-notes.18.3.

Belluso, E., Baronnet, A., Capella, S., 2020. Naturally occurring asbestiform minerals in Italian Western Alps and in other Italian sites. Environ. Eng. Geosci. 26, 39–46. https://doi.org/10.2113/EEG-2276.

Berger, V.I., Singer, D.A., Bliss, J.D., Moring, B.C., 2011. Ni-Co Laterite Deposits of the World - Database and Grade and Tonnage Models. Reston, Virginia.

Boffetta, P., Mundt, K.A., Thompson, W.J., 2018. The epidemiologic evidence for elongate mineral particle (EMP)-related human cancer risk. Toxicol. Appl. Pharmacol. 361, 100–106. https://doi.org/10.1016/j.taap.2018.09.021.

Butt, C.R.M., Cluzel, D., 2013. Nickel laterite ore deposits: weathered serpentinites. Elements 9, 123–128. https://doi.org/10.2113/gselements.9.2.123.

Campopiano, A., Bruno, M.R., Olori, A., Angelosanto, F., Iannò, A., Casciardi, S., Spadafora, A., 2018. Fibrous antigorite in Mount Reventino area of central Calabria. J. Mediterr. Earth Sci. 10, 17–25. https://doi.org/10.3304/JMES.2018.012.

Campopiano, A., Cannizzaro, A., Olori, A., Angelosanto, F., Bruno, M.R., Sinopoli, F., Bruni, B.M., Casalinuovo, F., Iavicoli, S., 2020. Environmental contamination by naturally occurring asbestos (NOA): analysis of sentinel animal lung tissue. Sci. Total Environ. 745, 140990. https://doi.org/10.1016/j.scitotenv.2020.140990.

Carbone, M., Baris, Y.I., Bertino, P., Brass, B., Comertpay, S., Dogan, A.U., Gaudino, G., Jube, S., Kanodia, S., Partridge, C.R., Pass, H.I., Rivera, Z.S., Steele, I., Tuncer, M., Way, S., Yang, H., Miller, A., 2011. Erionite exposure in North Dakota and Turkish villages with mesothelioma. Proc. Natl. Acad. Sci. 108, 13618–13623. https://doi.org/10.1073/pnas.1105887108/-/DCSupplemental.www.pnas.org/cgi/doi/10.1073/pnas.1105887108.

Case, B.W., Camus, M., Richardson, L., Parent, M.E., Désy, M., Siemiatycki, J., 2002. Preliminary findings for pleural mesothelioma among women in the Québec chrysotile mining regions. Ann. Occup. Hyg. 46, 128–131. https://doi.org/10.1093/annhyg/46.suppl_1.128.

Case, B.W., Abraham, J.L., Meeker, G.P., Pooley, F.D., Pinkerton, K.E., 2011. Applying definitions of "asbestos" to environmental and "low-dose" exposure levels and health effects, particularly malignant mesothelioma. J. Toxicol. Environ. Heal. - Part B Crit. Rev. 14, 3–39. https://doi.org/10.1080/10937404.2011.556045.

Cavallo, A., Petriglieri, J.R., 2020. Naturally occurring asbestos in Valmalenco (central Alps, northern Italy): from quarries and mines to stream sediments. Environ. Eng. Geosci. 26, 47–52. https://doi.org/10.2113/EEG-2270.

Cavallo, A., Rimoldi, B., 2013. Chrysotile asbestos in serpentinite quarries: a case study in Valmalenco, Central Alps. Northern Italy. Environ. Sci. Process. Impacts 15, 1341–1350. https://doi.org/10.1039/c3em00193h.

Chardon, D., Chevillotte, V., 2006. Morphotectonic evolution of the New Caledonia ridge (Pacific southwest) from post-obduction tectonosedimentary record. Tectonophysics 420, 473–491. https://doi.org/10.1016/j.tecto.2006.04.004.

Chevillotte, V., Chardon, D., Beauvais, A., Maurizot, P., Colin, F., 2006. Long-term tropical morphogenesis of New Caledonia (Southwest Pacific): importance of positive epeirogeny and climate change. Geomorphology 81, 361–375. https://doi.org/10.1016/j.geomorph.2006.04.020.

Cluzel, D., Vigier, B., 2008. Syntectonic mobility of supergene nickel ores of New Caledonia (Southwest Pacific). Evidence from garnierite veins and faulted regolith. Resour. Geol. 58, 161–170. https://doi.org/10.1111/j.1751-3928.2008.00053.x.

Cluzel, D., Aitchison, J.C., Picard, C., 2001. Tectonic accretion and underplating mafic terranes in the late Eocene intraoceanic fore-arc of New Caledonia (Southwest Pacific): geodynamic implications. Tectonophysics 340, 23–59. https://doi.org/10.1016/S0040-1951(01)00148-2.

Cluzel, D., Maurizot, P., Collot, J.Y., Sevin, B., 2012. An outline of the Geology of New Caledonia; from Permian-Mesozoic Southeast Gondwanaland active margin to Cenozoic obduction and supergene evolution. Episodes 35, 72–86.

Cluzel, D., Boulvais, P., Iseppi, M., Lahondère, D., Lesimple, S., Maurizot, P., Paquette, J.L., Tarantola, A., Ulrich, M., 2020. Slab-derived origin of tremolite–antigorite veins in a supra-subduction ophiolite: the Peridotite Nappe (New Caledonia) as a case study. Int. J. Earth Sci. 109, 171–196. https://doi.org/10.1007/s00531-019-01796-6.

Collot, J.Y., Malahoff, A., Recy, J., Latham, G., Missègue, F., 1987. Overthrust emplacement of New Caledonia ophiolite: geophysical evidence. Tectonics 6, 215–232. https://doi.org/10.1029/TC006i003p00215.

Di Giuseppe, D., Harper, M., Bailey, M., Erskine, B., Della Ventura, G., Ardit, M., Pasquali, L., Tomaino, G., Ray, R., Mason, H., Dyar, M.D., Hanuskova, M., Giacobbe, C., Zoboli, A., Gualtieri, A.F., 2019. Characterization and assessment of the potential toxicity/pathogenicity of fibrous glaucophane. Environ. Res. 178, 108723. https://doi.org/10.1016/j.envres.2019.108723.

DIMENC-SGNC, 2010. Cartographie des terrains potentiellement amiantifères en Nouvelle-Caléconie - Etat des connaissances, mars 2010.

Dogan, M., Emri, S., 2000. Environmental health problems related to mineral dusts in Ankara and Eskisehir, Turkey. Yerbilimleri 22, 149–161.

EPA, 2014. Toxicological review of Libby amphibole asbestos, Integrated Risk Information System, National Center for Environmental Assessment., Epa/635/R-11/002F. Washington, DC.

Erskine, B.G., Bailey, M., 2018. Characterization of asbestiform glaucophane-winchite in the Franciscan Complex blueschist, northern Diablo Range. California. Toxicol. Appl. Pharmacol. 361, 3–13. https://doi.org/10.1016/j.taap.2018.09.020.

Favero-Longo, S.E., Turci, F., Fubini, B., Castelli, D., Piervittori, R., 2013. Lichen deterioration of asbestos and asbestiform minerals of serpentinite rocks in Western Alps. Int. Biodeterior. Biodegrad. 84, 342–350. https://doi.org/10.1016/j.ibiod.2012.07.018.

Fitz Gerald, J.D., Eggleton, R.A., Keeling, J.L., 2010. Antigorite from Rowland Flat, South Australia: asbestiform character. Eur. J. Mineral. 22, 525–533. https://doi.org/10.1127/0935-1221/2010/0022-2045.

Fornero, E., Belluso, E., Capella, S., Bellis, D., 2009. Environmental exposure to asbestos and other inorganic fibres using animal lung model. Sci. Total Environ. 407, 1010–1018. https://doi.org/10.1016/j.scitotenv.2008.10.021.

Fritsch, E., Juillot, F., Dublet, G., Fandeur, D., Fonteneau, L., Martin, E., Auzende, A.L., Morin, G., Robert, J.L., Galoisy, L., Calas, G., Grauby, O., Boulvais, P., Cathelineau, M., 2014. Analyse fine des minerais latéritiques. Approche pétrographique, minéralogique, géochimique et isotopique., Gisements de Nickel latéritique de Nouvelle-Calédonie. Nouméa.

Fritsch, E., Bailly, L., Sevin, B., 2017. Atlas des latérites nickélifères de Nouvelle-Calédonie. Gisements de Nickel latéritique de Nouvelle-Calédonie, Nouméa.

Frost, B.R., Evans, K.A., Swapp, S.M., Beard, J.S., Mothersole, F.E., 2013. The process of serpentinization in dunite from New Caledonia. Lithos 178, 24–39. https://doi.org/10.1016/j.lithos.2013.02.002.

Garabrant, D.H., Pastula, S.T., 2018. A comparison of asbestos fiber potency and elongate mineral particle (EMP) potency for mesothelioma in humans. Toxicol. Appl. Pharmacol. 361, 127–136. https://doi.org/10.1016/j.taap.2018.07.003.

Gianfagna, A., Ballirano, P., Bellatreccia, F., Bruni, B.M., Paoletti, L., Oberti, R., 2003. Characterization of amphibole fibres linked to mesothelioma in the area of Biancavilla, Eastern Sicily. Italy. Mineral. Mag. 67, 1221–1229. https://doi.org/10.1180/0026461036760160.

Goldberg, P., Goldberg, M., Marne, M.J., Hirsch, A., Tredaniel, J., 1991. Incidence of pleural mesothelioma in New Caledonia: a 10-year survey (1978–1987). Arch. Environ. Health 46, 306–309. https://doi.org/10.1080/00039896.1991.9934393.

Groppo, C., Compagnoni, R., 2007. Ubiquitous fibrous antigorite veins from the Lanzo Ultramafic Massif, Internal Western Alps (Italy): characterisation and genetic conditions. Period. di Mineral. 76, 169–181. https://doi.org/10.2451/2007PM0014.

Groppo, C., Rinaudo, C., Cairo, S., Gastaldi, D., Compagnoni, R., 2006. Micro-Raman spectroscopy for a quick and reliable identification of serpentine minerals from ultramafics. Eur. J. Mineral. 18, 319–329. https://doi.org/10.1127/0935-1221/2006/0018-0319.

Gualtieri, A.F., Pollastri, S., Gandolfi, N.B., Ronchetti, F., Albonico, C., Cavallo, A., Zanetti, G., Marini, P., Sala, O., 2014. Determination of the concentration of asbestos minerals in highly contaminated mine tailings: an example from abandoned mine waste of Crètaz and Èmarese (Valle d'Aosta, Italy). Am. Mineral. 99, 1233–1247. https://doi.org/10.2138/am.2014.4708.

Gualtieri, A.F., Gandolfi, N.B., Passaglia, E., Pollastri, S., Mattioli, M., Giordani, M., Ottaviani, M.F., Cangiotti, M., Bloise, A., Barca, D., Vigliaturo, R., Viani, A., Pasquali, L., Gualtieri, M.L., 2018a. Is fibrous ferrierite a potential health hazard? Characterization and comparison with fibrous erionite. Am. Mineral. 103, 1044–1055. https://doi.org/10.2138/am-2018-6508.

Gualtieri, A.F., Gandolfi, N.B., Pollastri, S., Rinaldi, R., Sala, O., Martinelli, G., Bacci, T., Paoli, F., Viani, A., Vigliaturo, R., 2018b. Assessment of the potential hazard represented by natural raw materials containing mineral fibres—the case of the feldspar from Orani, Sardinia (Italy). J. Hazard. Mater. 350, 76–87. https://doi.org/10.1016/j.jhazmat.2018.02.012.

Gunter, M.E., 2018. Elongate mineral particles in the natural environment. Toxicol. Appl. Pharmacol. 361, 157–164. https://doi.org/10.1016/j.taap.2018.09.024.

Harper, M., 2008. 10th anniversary critical review: naturally occurring asbestos. J. Environ. Monit. 10, 1394–1408. https://doi.org/10.1039/b810541n.

IARC, 2012. Monographs on the evaluation of carcinogenic risks to humans. Arsenic, metals, fibres, and dusts. A review of human carcinogens., IARC Monographs on the Evaluation of Carcinogenic Risks to Humans. Lyon, France.

IARC, 2017. Monographs on the evaluation of carcinogenic risks to humans. Fluoro-edenite, silicon carbide fibres and whhiskers, and single-walled and multi-walled carbon nanotubes., IARC Monographs on the Evaluation of Carcinogenic Risks to Humans. Lyon, France.

Ingravalle, F., Ceballos, L.A., D'Errico, V., Mirabelli, D., Capella, S., Belluso, E., Pezzolato, M., Bozzetta, E., Dondo, A., Di Blasio, A., Meistro, S., Vizio, C., Fraccaro, E., Ardizzone, M., Seghesio, A., Ru, G., 2020. Wild rats as urban detectives for latent sources of asbestos contamination. Sci. Total Environ. 729. https://doi.org/10.1016/j.scitotenv.2020.138925.

Keeling, J.L., Raven, M.D., Self, P.G., Eggleton, R.A., 2008. Asbestiform antigorite occurrence in South Australia., in: 9th International Congress for Applied Mineralogy. ICAM 2008, 329–336.

Koumantakis, E., Kalliopi, A., Dimitrios, K., Gidarakos, E., 2009. Asbestos pollution in an inactive mine: determination of asbestos fibers in the deposit tailings and water. J. Hazard. Mater. 167, 1080–1088.

Lagabrielle, Y., Chauvet, A., Ulrich, M., Guillot, S., 2013. Passive obduction and gravity-driven emplacement of large ophiolitic sheets: the New Caledonia ophiolite (SW Pacific) as a case study? Bull. la Soc. Geol. Fr. 184, 545–556. https://doi.org/10.2113/gssgfbull.184.6.545.

Lahondère, D., 2007. L'amiante environnemental en Nouvelle Calédonie : expertise géologique des zones amiantifères. Evaluation des actions engagées. Nouméa, Nouvelle Calédonie. doi:BRGM/RP-55894-FR.

Lahondère, D., 2012. Serpentinisation et fibrogenèse dans les massifs de péridotite de Nouvelle-Calédonie. Atlas des occurrences et des types de fibres d'amiante sur mine, Nouméa, Nouvelle Calédonie.

Laporte-Magoni, C., Tribaudino, M., Meyer, M., Fubini, B., Tomatis, M., Juillot, F., Petriglieri, J.R., Gunkel-Grillon, P., Selmaoui-Folcher, N., 2018. Amiante et Bonnes Pratiques. Rapport Final, Nouméa, Nouvelle Calédonie.

Lee, R.J., Strohmeier, B.R., Bunker, K.L., Van Orden, D.R., 2008. Naturally occurring asbestos - a recurring public policy challenge. J. Hazard. Mater. 153, 1–21. https://doi.org/10.1016/j.jhazmat.2007.11.079.

Marchesi, C., Garrido, C.J., Godard, M., Belley, F., Ferré, E., 2009. Migration and accumulation of ultra-depleted subduction-related melts in the Massif du Sud ophiolite (New Caledonia). Chem. Geol. 266, 171–186. https://doi.org/10.1016/j.chemgeo.2009.06.004.

Marsh, E.E., Anderson, E.D., Gray, F., 2013. Nickel-cobalt laterites: a deposit model: chapter H in mineral deposit models for resource assessment., in: Mineral Deposit Models for Resource Assessment. U.S. Geological Survey, Reston, Virginia, pp. 1–38. doi: https://doi.org/10.3133/sir20105070H

McRae, M.E., 2020. Nickel.

Meeker, G.P., Bern, A.M., Brownfield, I.K., Lowers, H.A., Sutley, S.J., Hoefen, T.M., Vance, J.S., 2003. The composition and morphology of amphiboles from the Rainy Creek complex, near Libby. Montana. Am. Mineral. 88, 1955–1969. https://doi.org/10.2138/am-2003-11-1239.

Mothersole, F.E., Evans, K.A., Frost, B.R., 2017. Abyssal and hydrated mantle wedge serpentinised peridotites: a comparison of the 15°20′N fracture zone and New

Caledonia serpentinites. Contrib. to Mineral. Petrol. 172, 1–25. https://doi.org/10.1007/s00410-017-1381-x.
NIOSH, 2011. Asbestos fibers and other elongate mineral particles: state of the science and roadmap for research., Current Intelligence Bulletin 62.
Orloff, O., Gonord, H., 1968. Note préliminaire sur un nouveau complexe sédimentaire continental situé sur les massifs du Goa N'Doro et de Kadjitra (région côtière à l'Est de la Nouvelle-Calédonie), définition de la formation et conséquences de cette découverte sur l'âge des fractures. Comptes Rendus l'Académie des Sci. 267, 5–8.
Pelletier, B., 1996. Serpentine in nickel silicate ore from New Caledonia. Nickel '96 Miner. to Mark. 197–205.
Petriglieri, J.R., Salvioli-Mariani, E., Mantovani, L., Tribaudino, M., Lottici, P.P., Laporte-Magoni, C., Bersani, D., 2015. Micro-Raman mapping of the polymorphs of serpentine. J. Raman Spectrosc. 46, 953–958. https://doi.org/10.1002/jrs.4695.
Petriglieri, J.R., Laporte-Magoni, C., Gunkel-Grillon, P., Tribaudino, M., Bersani, D., Sala, O., Le Mestre, M., Vigliaturo, R., Bursi Gandolfi, N., Salvioli-Mariani, E., 2020a. Mineral fibres and environmental monitoring: a comparison of different analytical strategies in New Caledonia. Geosci. Front. 11, 189–202. https://doi.org/10.1016/j.gsf.2018.11.006.
Petriglieri, J.R., Laporte-Magoni, C., Salvioli-Mariani, E., Tomatis, M., Gazzano, E., Turci, F., Cavallo, A., Fubini, B., 2020b. Identification and preliminary toxicological assessment of a non-regulated mineral fiber: fibrous antigorite from New Caledonia. Environ. Eng. Geosci. XXVI, 89–97. doi:https://doi.org/10.2113/EEG-2274
Pirard, C., Hermann, J., O'neill, H.S.C., 2013. Petrology and geochemistry of the crust-mantle boundary in a Nascent Arc, Massif du Sud Ophiolite, New Caledonia, SW Pacific. J. Petrol. 54, 1759–1792. https://doi.org/10.1093/petrology/egt030.
Quesnel, B., 2015. Alteration supergene, circulation des fluides et deformation interne du mas- sif de Koniambo, Nouvelle-Caledonie: implication sur les gisements nickeliferes lateritiques. Universite Rennes 1. doi:NNT:2015REN1S103.
Quesnel, B., Gautier, P., Cathelineau, M., Boulvais, P., Couteau, C., Drouillet, M., 2016. The internal deformation of the Peridotite Nappe of New Caledonia: a structural study of serpentine-bearing faults and shear zones in the Koniambo Massif. J. Struct. Geol. 85, 51–67. https://doi.org/10.1016/j.jsg.2016.02.006.
Ribeiro Da Costa, I., Barriga, F.J.A.S., Viti, C., Mellini, M., Wicks, F.J., 2008. Antigorite in deformed serpentinites from the Mid-Atlantic Ridge. Eur. J. Mineral. 20, 563–572. https://doi.org/10.1127/0935-1221/2008/0020-1808.
Rinaudo, C., Gastaldi, D., Belluso, E., 2003. Characterization of chrysotile, antigorite, and lizardite by FT-Raman spectroscopy. Can. Mineral. 41, 883–890. https://doi.org/10.2113/gscanmin.41.4.883.
Robb, L., 2010. Introduction to Ore-forming Processes. John Wiley & Sons.
Rogers, A.J., 2018. Exposures estimates of the Wittenoom mining workforce and town residents–implications associated with risk estimation for persons exposed to asbestiform riebeckite. Toxicol. Appl. Pharmacol. 361, 168–170.
Rooney, J.S., Tarling, M.S., Smith, S.A.F., Gordon, K.C., 2018. Submicron Raman spectroscopy mapping of serpentinite fault rocks. J. Raman Spectrosc. 49, 279–286. https://doi.org/10.1002/jrs.5277.
Sullivan, P.A., 2007. Vermiculite, respiratory disease, and asbestos exposure in Libby. Montana: update of a cohort mortality study. Environ. Health Perspect. 115, 579–585. https://doi.org/10.1289/ehp.9481.
Tarling, M.S., Rooney, J.S., Viti, C., Smith, S.A.F., Gordon, K.C., 2018. Distinguishing the Raman spectrum of polygonal serpentine. J. Raman Spectrosc., 1–7 https://doi.org/10.1002/jrs.5475.
Troly, G., Esterle, M., Pelletier, B., Reibell, W., 1979. Nickel deposits in New Caledonia, some factors influencing their formation., in: International Laterite Symposium. American Institute of Mining Metallurgy and Petroleum Engineering Society, New Orleans, pp. 85–119.
Trotet, F., 2012. Fibrous serpentinites in oxyded nickel ores from New Caledonia: risk management in a modern mining company - societal implications., in: Serpentine Days. p. 87.
Turci, F., Favero-Longo, S.E., Gazzano, C., Tomatis, M., Gentile, L., Bergamini, M., 2016. Assessment of asbestos exposure during a simulated agricultural activity in the proximity of the former asbestos mine of Balangero. Italy. J. Hazard. Mater. 308, 321–327. https://doi.org/10.1016/j.jhazmat.2016.01.056.
Turci, F., Tomatis, M., Pacella, A., 2017. Surface and bulk properties of mineral fibres relevant to toxicity. In: Gualtieri, A.F. (Ed.), Mineral Fibres: Crystal Chemistry. Chemical Physical Properties, Biological Interaction and Toxicity EMU Notes in Mineralogy. European Mineralogical Union and the Mineralogical Society of Great Britain & Ireland, pp. 171–214.
Ulrich, M., Picard, C., Guillot, S., Chauvel, C., Cluzel, D., Meffre, S., 2010. Multiple melting stages and refertilization as indicators for ridge to subduction formation: the New Caledonia ophiolite. Lithos 115, 223–236. https://doi.org/10.1016/j.lithos.2009.12.011.
Vignaroli, G., Belardi, G., Serracino, M., 2013. Multi-scale geological evaluation for quarrying activities in ophiolitic rocks: implications for asbestos-related legislation. Bull. Eng. Geol. Environ. 72, 285–302. https://doi.org/10.1007/s10064-013-0475-6.
Villanova-de-Benavent, C., Proenza, J.A., Galí, S., García-Casco, A., Tauler, E., Lewis, J.F., Longo, F., 2014. Garnierites and garnierites: textures, mineralogy and geochemistry of garnierites in the Falcondo Ni-laterite deposit. Dominican Republic. Ore Geol. Rev. 58, 91–109. https://doi.org/10.1016/j.oregeorev.2013.10.008.
Villanova-De-Benavent, C., Nieto, F., Viti, C., Proenza, J.A., Galí, S., Roqué-Rosell, J., 2016. Ni-phyllosilicates (garnierites) from the Falcondo Ni-laterite deposit (Dominican Republic): mineralogy, nanotextures, and formation mechanisms by HRTEM and AEM. Am. Mineral. 101, 1460–1473. https://doi.org/10.2138/am-2016-5518.
Viti, C., 2010. Serpentine minerals discrimination by thermal analysis. Am. Mineral. 95, 631–638. https://doi.org/10.2138/am.2010.3366.
Vortisch, W., Baur, X., 2018. Asbestiform antigorite: a dangerous mineral in serpentinites. A plea to treat asbestiform antigorite as an asbestos group mineral in terms of its occupational health safety effects. Neues Jahrb. fur Mineral. Abhandlungen 195, 41–64. https://doi.org/10.1127/njma/2017/0070.
Wells, M.A., Ramanaidou, E.R., Verrall, M., Tessarolo, C., 2009. Mineralogy and crystal chemistry of "garnierites" in the Goro lateritic nickel deposit, New Caledonia. Eur. J. Mineral. 21, 467–483. https://doi.org/10.1127/0935-1221/2009/0021-1910.
WHO, 1997. Determination of Airborne Fibre Number Concentrations. A Recommended Method, by Phase-contrast Optical Microscopy (Membrane Filter Method). Geneva. doi:ISBN 92 4 154496 1.
Wicks, F.J., Whittaker, E.J.W., 1977. Serpentine texture and serpentinization. Can. Mineral. 15, 459–488.